NIH Public Access
Author Manuscript
Stem Cells. Author manuscript; available in PMC 2014 December 01.

Published in final edited form as:
Stem Cells. 2013 December ; 31(12): 2737–2746. doi:10.1002/stem.1409.

MiR-133b promotes neural plasticity and functional recovery after treatment of stroke with multipotent mesenchymal stromal cells in rats via transfer of exosome-enriched extracellular particles

Hongqi Xin[1], **Yi Li**[1], **Zhongwu Liu**[1], **Xinli Wang**[1], **Xia Shang**[1], **Yisheng Cui**[1], **Zheng Gang Zhang**[1], and **Michael Chopp**[1,2]

[1]Department of Neurology, Henry Ford Hospital, Detroit, MI 48202

[2]Department of Physics, Oakland University, Rochester, MI 48309

Abstract

To test, *in vivo*, the hypothesis that exosomes from multipotent mesenchymal stromal cells (MSCs) mediate microRNA 133b (miR-133b) transfer which promotes neurological recovery from stroke, we employed knock-in and knock-down technologies to up-regulate or down-regulate the miR-133b level in MSCs (miR-133b$^+$MSCs or miR-133b$^-$MSCs) and their corresponding exosomes, respectively. Rats were subjected to middle cerebral artery occlusion (MCAo) and were treated with naïve MSCs, miR-133b$^+$MSCs, or miR-133b$^-$MSC at one day after MCAo. Compared with controls, rats receiving naïve MSC treatment significantly improved functional recovery, and exhibited increased axonal plasticity and neurite remodeling in the ischemic boundary zone (IBZ) at day 14 after MCAo. The outcomes were significantly enhanced with miR-133b$^+$MSC treatment, and were significantly decreased with miR-133b$^-$MSC treatment, compared to naïve MSC treatment. The miR-133b level in exosomes collected from the cerebral spinal fluid was significantly increased after miR-133b$^+$MSC treatment, and was significantly decreased after miR-133b$^-$MSC treatment at day 14 after MCAo, compared to naïve MSC treatment. Tagging exosomes with green fluorescent protein demonstrated that exosomes-enriched extracellular particles were released from MSCs and transferred to adjacent astrocytes and neurons. The expression of selective targets for miR-133b, connective tissue growth factor and *ras* homolog gene family member A, were significantly decreased in the IBZ after miR-133b$^+$MSC treatment, while their expression remained at similar elevated levels after miR-133b$^-$MSC treatment, compared to naïve MSC treatment. Collectively, our data suggest that exosomes from MSCs mediate the miR-133b transfer to astrocytes and neurons, which regulate gene expression, subsequently benefit neurite remodeling and functional recovery after stroke.

Contact: Michael Chopp, Ph.D. Professor and Vice Chair, Department of Neurology in Henry Ford Hospital, 2799 West Grand Blvd. Detroit, MI 48202, Tel: 313-916-3936 Fax: 313-916-1318 chopp@neuro.hfh.edu.

Author Contribution:
Hongqi Xin: Conception and design, Collection and/or assembly of data, Data analysis and interpretation, Manuscript writing
Yi Li: Conception and design, Data analysis and interpretation, Financial support, Manuscript writing
Zhongwu Liu: Collection and/or assembly of data
Xinli Wang: Collection and/or assembly of data
Xia Sang: Collection and/or assembly of data
Yisheng Cui: Collection and/or assembly of data
Zheng Gang Zhang: Conception and design, Data analysis and interpretation
Michael Chopp: Conception and design, Data analysis and interpretation, Financial support, Manuscript writing, Final approval of manuscript

Disclosure of potential conflicts of interest
None

NIH-PA Author Manuscript
NIH-PA Author Manuscript
NIH-PA Author Manuscript

NIH-PA Author Manuscript

NIH-PA Author Manuscript

NIH-PA Author Manuscript

Keywords

microRNA 133b; exosomes; multipotent mesenchymal stromal cells; neurite remodeling; stroke

Introduction

In eukaryotic cells, micro RNAs (miRNAs) constitute a major regulatory gene family [1–4]. The human genome may encode over 1000 miRNAs [3] which target about 60% of mammalian genes [5, 6] and are abundant in many human cell types [7]. By affecting gene expression, miRNAs are likely involved in most biological processes [8–12]. The function of individual miRNAs is just beginning to emerge in mature neurons, while the role of miRNAs at various stages of neuronal development and maturation has been recently elucidated [13–15]. Numerous miRNAs are expressed in spatially and temporally controlled manners in the nervous system [16–21], consistent with the hypothesis that miRNAs have important roles in the gene regulatory networks involved in adult neural plasticity [17, 22–24].

Exosomes are membrane vesicles that contain RNA molecules including messenger RNAs (mRNAs) and miRNAs, which can be transferred between cells and thus affect the protein production of recipient cells [25–27]. Increasing evidence indicates that exosomes play an important role in cell-to-cell communication [28–32]. In the nervous system, exosomes mediate cell-cell communication including the transfer of synaptic proteins, mRNAs and microRNAs [29]. Those exosomes either act locally within the presynaptic terminal or are transported back to presynaptic neuronal cell bodies and are associated with learning and memory [29].

Multipotent mesenchymal stromal cells (MSCs) have potential therapeutic benefit in many diseases including neurological diseases, injury and stroke [33–40]. Our previous *in vitro* studies demonstrate that the miR-133b is significantly increased in exosomes from MSCs exposed to ischemic cerebral extracts, and the miR-133b is transferred via exosomes to astrocytes and neurons, which subsequently increase neurite outgrowth [41]. In the present study, we employed knock-in or knock-down technologies to up-regulate or down-regulate the miR-133b level in MSCs (miR-133b$^+$MSCs or miR-133b$^-$MSCs) and their corresponding exosomes, respectively, as gain or loss of miR-133b function experiments, and then administered these MSCs to rats subjected to middle cerebral artery occlusion (MCAo), to test whether *in vivo* the exosomes mediate miR-133b transfer to neural cells and subsequently promote neurite remodeling and functional recovery after MCAo.

Material and methods

All experimental procedures were carried out in accordance with the National Institutes of Health (NIH) Guide for the Care and Use of Laboratory Animals and approved by the Institutional Animal Care and Use Committee of Henry Ford Hospital.

MSC cultures and lentiviral production for miR-133b knocked-in or knocked-down MSCs

Bone marrow from male Wistar rats was mechanically dissociated, and the cells were washed and suspended in culture medium. Three days later, cells that tightly adhered to the plastic flasks were considered as P0 MSCs [42–44]. MSCs were cultured with α-modified MEM medium (Hyclone, Logan, UT) containing 20% fetal bovine serum (FBS, Gibco Laboratory, Grand Island, NY) and penicillin-streptomycin on 75 cm^2 tissue culture flasks (Corning St. Louis, MO) and 3~4 passages (P3~4) were used for lentivirus infection. MSCs were passaged or collected for injection when they achieved 80%-90% confluence. For the exosome isolation, we replaced conventional culture medium with an exosome depleted

NIH-PA Author Manuscript

NIH-PA Author Manuscript

NIH-PA Author Manuscript

FBS (EXO-FBS-250A-1, System Biosciences, Inc. Mountain View, CA) medium when the cells reached 60%-80% confluence. Followed by an additional 24hrs of culturing and the media were then collected for centrifugation.

We packaged the lentiviruses which contain the vectors of LentimiRa-GFP-hsa-miR-133b Vector (mh10170, Applied Biological Materials Inc., Richmond, BC, V6V 2G2 CANADA, pre-miR-133b inserted for miR-133b knock-in), pLenti-III-miR-GFP Control Vector (m001, Applied Biological Materials Inc., vector for miR-133b knock-in control), miRZip-133b anti-miR-133b microRNA construct (MZIP133b-PA-1, System Biosciences, Inc., miR-133b inhibitor inserted for miR-133b knock-down) and pGreenPuro Scramble Hairpin Control Construct (MZIP000-PA-1, System Biosciences, Inc., vector for miR-133b knock-down control), respectively, according to the manufacturer's suggested protocol. We then infected the primary cultured MSCs with these lentiviruses, to generate miR-133b knocked-in or knocked-down MSCs, respectively. The infection efficiency was monitored by the green fluorescent protein (GFP), and puromycin was used for selection of stable cell lines. The four stable MSC cell lines generated were identified as: miR-133b^{+}MSC, miR-133b^{+CON}MSC, miR-133b^{-}MSC and miR-133b^{-CON}MSC, respectively.

MCAo model

Adult male Wistar rats (weighing 270–300 g, n=51) purchased from Charles River (Wilmington, MA, USA) were subjected to right MCAo using a method of intraluminal vascular occlusion as modified in our laboratory [34]. Briefly, rats were initially anesthetized with 3.5% isoflurane and maintained with 1.0–2.0% isoflurane in 70% N_2O and 30% O_2 using a face mask. Rectal temperature was maintained at 37°C throughout the surgical procedure using a feedback regulated water heating system. A length of 4-0 monofilament nylon suture (18.5–19.5 mm), determined by the animal weight, with its tip rounded by heating near a flame, was advanced from the external carotid artery into the lumen of the internal carotid artery until it blocked the origin of the MCA. Two hours (h) after MCAo, animals were re-anesthetized with isoflurane and reperfusion was performed by withdrawal of the suture until the tip cleared the lumen of the external carotid artery. Immunosuppressants were not used in any animals in this study.

MSC administration

At 24 h post ischemia, randomly selected rats (n=6/group, n=36 in total) received naive MSC, miR-133b^{+}MSC, miR-133b^{+CON}MSC, miR-133b^{-}MSC and miR-133b^{-CON}MSC or vehicle administration. Approximately 3×10^{6} MSCs in 1 ml phosphate-buffered saline (PBS) or PBS alone was slowly injected via the tail vein over a 5 minute (min) period into each rat. Behavioral tests, including the adhesive-removal test (used to measure somatosensory deficits [33, 45, 46]) and the Foot-fault test (used to measure forelimb dysfunction [33, 46, 47]), were performed at day 1 post MCAo immediately prior to the treatment, and at days 3, 7 and 14 after MCAo. All rats were sacrificed at 14 days after MCAo. To test the corresponding miR-133b level in the exosomes released in the cerebral spinal fluid (CSF), CSF samples were acquired immediately prior to sacrifice. At the end of the experiment, rats were deeply anesthetized with a Ketamine (160 mg/kg) and Xylazine (26 mg/kg) mixture intraperitoneally, and were transcardially perfused with heparinized saline. Rat brains were snapped frozen in liquid nitrogen, and stored in −80°C. A standard frozen block (within the center of the lesion of MCAo), corresponding to coronal coordinates bregma −2.0~2.0 mm was obtained from which a series of 40μm-thickness were performed for molecular studies (Western blot and RT-PCR) and 8μm-thickness for histochemistry and immunostaining.

NIH-PA Author Manuscript

NIH-PA Author Manuscript

NIH-PA Author Manuscript

MSC exosome isolation

The exosome isolation was performed at 4°C, as previously described [48, 49]. Briefly, the supernatants collected from cultured MSCs or the CSF (diluted with 20mM HEPES) were first filtered through a 0.2 μm filter to remove large debris and dead cells. Small cell debris was removed by centrifugation at 100,000×g for 30 min, and then the resulting supernatants were further centrifuged at 100,000 ×g for 3 h. By this step, the pellets primarily contained exosomes [49]. For purification of the exosomes, the pellets containing exosomes were resuspended in 0.25 M sucrose buffered with 20mM HEPES, pH 7.4, and loaded onto a sucrose step gradient (2.5, 2.25, 2.0, 1.75, 1.5, 1.25, 1.0, 0.75, and 0.5 M). The sucrose gradient was then centrifuged at 100,000 ×g for 5 h and 10 fractions were collected and diluted with 20 mM HEPES, pH 7.4, and re-centrifuged at 100,000 ×g for 1.5 h. Exosomes can be identified by the marker proteins, CD63 [50, 51] or Alix [52–54], using Western blot, as well as by electron microscopy to verify the exosome presence [55, 56]. The final exosome pellets harvested from 1×10^7 cells were identified as previously described [41] and resuspended in 30 to 50 μl of PBS and stored at −80°C for further use.

MiRNA assay

For the measurement of miR-133b in exosomes from the CSF and cultured cells, samples were lysed in Qiazol reagents and the total RNA was isolated using the miRNeasy Mini kit (Qiagen, Valencia, CA). By RT-PCR, we detected the miR-133b level. Briefly, miRNAs were reverse transcribed with the miRNA Reverse Transcription kit (Applied Biosystems, Foster City, CA) and PCR amplifcation was performed with the TaqMan miRNA assay kit (Applied Biosystems, which is specific for mature miRNA sequences) according to the manufacturer`s protocols, with U6 snRNA as an internal control.

Biotinylated dextran amine (BDA) label for detection of axonal plasticity

BDA (3,000 Da, 10% solution in PBS; Invitrogen, Carlsbad, CA) was employed to retrogradely label pyramidal neurons in additional rats subjected to MCAo following previously described procedures [40]. Briefly, additional MCAo rats (n=3/group, n=12 in total) were treated with PBS, naive MSCs, miR-133b$^+$MSCs, or miR-133b$^-$MSCs (3×10^6, respectively) via tail vein injection at 1 day after MCAo, and 100 nl of BDA was injected into the contralateral pyramidal tract at the medulla level at 7 days before sacrifice. At day 14 after MCAo, animals were transcardially perfused with saline and 4% paraformaldehyde. The cervical spinal cord segments of C1 and C4 to 6 were processed for vibratome traverse section (75 μm). Sections were incubated with 0.5% H_2O_2 for 20 minutes followed with avidinbiotin-peroxidase complex (Vector Laboratories, Burlingame, Calif) at 4°C for 48 h, and BDA-labeled axons were visualized with 3, 3'-Diaminobenzidine (DAB) for light microscopy examination. Subsequently, BDA positive labeling axonal densities in the ipsilateral area were quantitatively measured as the indicator of axonal plasticity.

Histochemistry and immunostaining

To address the neurite remodeling in the ischemic boundary zone (IBZ), Bielshowsky silver (a marker of neuronal fibers) histochemistry staining and neurofilament heavy 200 kDa (NF-200, a marker for apical dendrites of large cortical pyramidal neurons [57, 58]) immunostaining and synaptophysin (a marker for synapses, since synaptophysin is ubiquitously present at the synapses [59]) immunostaining were employed, respectively. Briefly, for histochemistry staining, 8μm-thickness frozen brain slides were placed in 20% silver nitrate in the dark, then ammonium hydroxide was added to stain the slides until the tissues turned brown with a gold background and they were then treated with sodium thiosulfate. For immunostaining, adjacent frozen brain sections were incubated with the

NIH-PA Author Manuscript

NIH-PA Author Manuscript

NIH-PA Author Manuscript

primary antibodies against NF-200 (dilution 1:500, Abcam, ab82259) and synaptophysin (dilution 1:100, Chemicon, MAB5258), followed with corresponding horseradish peroxidase (HRP) conjugated to secondary antibodies and DAB developing, respectively. Positive staining within 9 areas (4 from the cortex, 4 from the striatum and 1 from the corpus callosum) selected along the IBZ in these groups was measured using a light microscope [60]. The MicroComputer Imaging Device (MCID) software was used to analyze the integrated density of positive staining signal within the IBZ.

Expression of GFP-tagged CD63 in MSCs and exosome secretion and uptake

MSCs were cultured overnight in six-well plates to 60 to 70% confluence, then transfected with 4 μg/well of purified pCT-CD63-GFP (CYTO120-PA-1, System Biosciences, Inc. Mountain View, CA) by using lipofectamine 2000 (11668-019, Invitrogen, Carlsbad, CA) reagent, as recommended by the manufacturer. Cells were selected with 10 μg/mL puromycin dihydrochloride (A11138-03, Invitrogen, Carlsbad, CA) for three weeks. Puromycin resistant and GFP positive cells were further isolated, expanded and maintained in the selection medium as long as the cells were in culture. The expression of GFP-CD63 in the selected cell lines, herein referred to as CD63-GFP-MSCs, was verified by immunoblotting and immunofluorescence. Another group of rats (n=3) subjected to MCAo were administered with these CD63-GFP-MSCs at 24 h post stroke. At 14 days after MCAo, rats were deeply anesthetized with a Ketamine and Xylazine and transcardially perfused with heparinized saline. Rat brains were snapped frozen in liquid nitrogen, and stored at −80°C. The 8-μm-thick frozen brain sections corresponding to coronal coordinates bregma −1.0~1.0 mm [61] were generated as noted above, and immunofluorescent staining was employed to distinguish astrocytes and neurons with glial fibrillary acidic protein (GFAP, dilution 1:10000, Dako Z0334; Dako, Carpinteria, CA) and microtubule-associate protein 2 (MAP-2 for neuronal dendrites, dilution 1:200, Sigma, St. Louis, MO) followed with corresponding Cy3-conjugated secondary antibodies, respectively. A laser scanning confocal microscope was employed to examine the secretion of exosomes from GFP tagged MSCs and the up-take of exosomes by astrocytes and neurons.

Statistical analysis

Data are expressed as means±SE. The differences between mean values were evaluated with the two tailed Student's t-test (for 2 groups) by the computer programs Microsoft Excel 2000 (Microsoft, Redmond, WA). The Global test using the Generalized Estimating Equation (GEE) was employed to evaluate the MSC treatment effects influenced by miR133b on functional recovery [62, 63]. Repeated measures analysis was used to evaluate data with repeated measurements over time (e.g. functional tests) or histological evaluation on multiple regions per subject. Analysis began testing for the factor interaction, followed by testing the main factor effect if no interaction was detected at 0.05 level, and/or a sub-group analysis, if the interaction or main effect was detected at 0.05 level [64].

Results

Lentivirus modified miR-133b level in MSCs and corresponding exosomes

Puromycin selected stable MSC cell lines were infected with LentimiRa-GFP-hsa-mir-133b lentivirus (miR-133b^{+}MSC), GFP Blank miRNA/microRNA lentivirus (miR-133b^{+CON}MSC), miRZip-133b anti-miR-133b microRNA lentivirus (miR-133b^{-}MSC) and pGreenPuro Scramble Hairpin Control lentivirus (miR-133b^{-CON}MSC), respectively. GFP was used to monitor the infection efficiency (Fig 1A). RT-PCR data show that the miR-133b expression level in miR-133b^{+}MSCs and in their exosomes was significantly increased compared to those in miR-133b^{+CON}MSCs, and miR-133b expression level was significantly decreased in miR-133b^{-}MSCs and in their

NIH-PA Author Manuscript

NIH-PA Author Manuscript

NIH-PA Author Manuscript

exosomes compared to those in miR-133b^{-CON}MSCs (Fig 1B). These data indicate that lentivirus systems containing the pre-miR133b or anti-miR-133b inhibitor successfully increase or decrease miR-133b levels in the MSCs and their exosomes, respectively.

To test whether miR-133b knock-in or knock-down affects the cell characteristics of MSCs, such as proliferation, we seeded 1×10^4 miR-133b$^+$MSCs and miR-133b$^-$MSCs as well as their corresponding control miR-133b^{+CON}MSCs and miR-133b^{-CON}MSCs into 24-well plates. These cells were conventionally cultured for 7 days, and the cell numbers were counted to perform cell growth curve analysis. We calculated the growth rate of each cell type by counting the total numbers of the cells in triplicate wells every day until 7days. Data showed that there were no significant differences in proliferation among the four types of cells (Fig 1C). Since miR-133b$^+$MSCs and miR-133b$^-$MSCs have the GFP tag, we also counted the GFP positive cell numbers under a fluorescent microscope at 14 days after MCAo in the IBZ (Fig 1D). There were no significant differences of the two types of cells in the IBZ (Fig 1E). These data indicate that the two cell lines have similar proliferation, survival and trafficking to the brain.

MiR-133b mediates MSC induced functional recovery

Rats subjected to 2 h MCAo, received PBS, naive MSCs and 4 types of modified MSCs (3×10^6/rats) intravenously at 24 h after MCAo (n=6/group). The adhesive-removal test (Fig 2A) and Foot-fault test (Fig 2B) were performed prior to the treatment after MCAo (baseline), at day 3 and 7, and at day 14 before sacrifice after MCAo. Compared with PBS treatment, naive MSCs, miR-133b^{+CON}MSCs and miR-133b^{-CON}MSCs significantly improved functional recovery (adhesive-removal and Foot-fault) at day 14 after MCAo, while miR-133b$^+$MSCs significantly improved functional recovery at day 7 (adhesive-removal test only) and day 14 (adhesive-removal and Foot-fault) after MCAo, and miR-133b$^-$MSCs had no obvious beneficial effects at these two time points. Compared with their corresponding control MSC treatments, miR-133b$^+$MSCs significantly improved, but miR-133b$^-$MSCs treatment significantly decreased, functional recovery (adhesive-removal and Foot-fault) at day 14 after MCAo. These data suggest that increased miR-133b expression in MSCs and in their released exosomes enhances functional recovery after stroke.

MiR-133b increases axonal plasticity and neurite remodeling in the IBZ

BDA (3000 Da) was employed to retrogradely label pyramidal neurons in rats subjected to MCAo. A representative image shows the BDA-positive labeling in a rat brain (Fig 3A). The BDA labeled axons in the caudal forelimb area (CFA) of ipsilateral side (Fig 3B) to the lesion were quantitatively measured using Image J (NIH Image), Data are shown as percentage of proportional areas [65]. Intracortical axonal density was significantly increased after naive MSC treatment compared with PBS treatment at day 14 after MCAo (Fig 3C). MiR-133b$^+$MSC treatment significantly increased but miR-133b$^-$MSC treatment significantly decreased the cortical axonal density at day 14 after MCAo compared with naive MSC treatment (Fig 3C), suggesting a role of MSC miR-133b in promoting axonal plasticity after stroke.

Frozen coronal sections were used for Bielshowsky silver, NF-200 and synaptophysin staining, respectively. Arrows indicate Bielshowsky silver, NF-200 and synaptophysin staining in the IBZ (3D, 3G and 3J, respectively) of the ipsilateral cortex (3E, 3H and 3K are enlarged from 3D, 3G, and 3J, respectively). Compared with PBS treatment (MCAo), the positive areas of Bielshowsky silver (3F), NF-200 (3I) and synaptophysin (3L) staining significantly increased at day 14 after MCAo along the IBZ after naive MSC treatment. MiR-133b$^+$MSC treatment significantly increased, but miR-133b$^-$MSC treatment

NIH-PA Author Manuscript

NIH-PA Author Manuscript

NIH-PA Author Manuscript

significantly decreased the positive areas of Bielshowsky silver, NF-200 and synaptophysin staining at day 14 after MCAo compared with naive MSC treatment. These data suggest that miR-133b increases neurite remodeling in the IBZ *in vivo*.

MiR-133b is increased in CSF exosomes and MSC exosomes are transferred to astrocytes and neurons

RT-PCR was employed to measure the miR-133b level in exosomes collected from the CSF at day 14 after MCAo (Fig 4A). Our data show that MCAo decreased the miR-133b level in the CSF exosomes. Treatment with naive MSCs significantly increased miR-133b level in the CSF exosomes compared to the MCAo control. MiR-133b^{+}MSC treatment further significantly increased miR-133b level in the CSF exosomes while miR-133b^{-}MSCs treatment significantly decreased the miR-133b level in the CSF exosomes, compared with the naive MSC treatment, respectively. These data suggest that the miR-133b increase in MSC exosomes evoked a miR-133b increase in the CSF.

To test the hypothesis that the exosomes mediate cell-cell communication between MSCs and neural cells, we transfected MSCs with the plasmid containing CD63-GFP fusion protein gene and treated rats subjected to MCAo with these CD63-GFP-MSCs. CD63 is a surface protein employed as a common marker of exosomes [66], CD63-GFP was visualized in exosomes using a laser scanning confocal microscope. As shown in Fig 4B and 4C, exosomes released from MSCs (arrows) in the IBZ were detected in adjacent astrocytes and neurons (arrow heads).

MiR-133b regulates the connective tissue growth factor (CTGF) expression in astrocytes and the *ras* homolog gene family member A (RhoA) expression in the IBZ

Immunostaining showed CTGF expression in the IBZ (Fig 5A) co-localized with GFAP (Fig 5B). Immunostaining analysis data showed that CTGF expression significantly increased in the IBZ at day 14 after MCAo compared with that in the normal rats. Administration of naive MSCs significantly decreased the CTGF expression in the IBZ at day 14 after MCAo. Compared with the naive MSC treatment, miR-133b^{+}MSC treatment significantly decreased CTFG expression at day 14 after MCAo, while miR-133b^{-}MSC treatment was sustained at a significantly elevated CTGF expression level in the IBZ at day 14 after MCAo (Fig 5C). These data indicate that miR-133b regulates CTGF expression in astrocytes. Western blot was used to detect the RhoA level in the ipsilateral brain tissue (Fig 5D), with the internal control protein glyceraldehyde 3-phosphate dehydrogenase (GAPDH). The data showed that RhoA expression significantly increased at day 14 after MCAo compared with normal rats. Naive MSC treatment significantly decreased the RhoA expression at day 14 after MCAo. MiR-133b^{+}MSC treatment further significantly decreased RhoA at day 14 after MCAo compared with that after naive MSC treatment, and the RhoA expression after miR-133b-MSC treatment was sustained at a similar elevated level at day 14 after MCAo compared with naive MSC treatment (Fig 5E). These data indicate that RhoA expression is regulated by miR-133b.

Discussion

MSCs enhance functional recovery in experimental stroke models [33, 64–66]. After stroke, only a very small percentage of injected MSCs enter the brain which may facilitated by the disruption of the blood-brain barrier [33, 67, 68]. The mechanisms underlying how the relatively few injected MSCs now resident in brain drive the robust functional recovery after stroke are not fully understood. Our prior *in vitro* studies identified a new mechanism that may underlie the therapeutic benefits of MSC-based therapies, that is, MSCs release exosomes which mediate the miRNA transfer from MSCs to parenchymal cells and thereby modulate

NIH-PA Author Manuscript

NIH-PA Author Manuscript

NIH-PA Author Manuscript

the neural cell gene expression and protein production which enhance neurite outgrowth [41]. In the present *in vivo* study, we demonstrate for the first time that, via exosome-enriched extracellular particles, the therapeutic benefit of MSC treatment of stroke is mediated by miRNA transfer, represented by miR-133b, to neural cells which evoke neurite remodeling and brain plasticity and subsequently benefit functional recovery.

Our previous RT-PCR [41] and in situ hybridization studies (see the Supplementary figure) showed that miR-133b levels in the IBZ of rats subjected to MCAo significantly increased after treatment with MSCs, and double immunostaining showed the miR-133b present in neurons and astrocytes. Our present data show that miR-133b levels in the CSF were correspondingly altered with the miR-133b level changes in MSCs administered to rats. GFP tagged exosome experiments also confirmed that MSC exosome-enriched particles are present in neurons/astrocytes. In conjunction with our previous *in vitro* data that miR-133b is mostly encapsulated within the MSC exosomes and MSC exosome treatment increased the miR-133b levels in neurons/astrocytes [41]. The present *in vivo* study thus indicates that the transfer of miR-133b from MSCs to neurons/astrocytes is likely mediated by exosomes. The question is, how do the exosomes released by MSCs enter the CSF? We consider the possibility that the exosomes produced by the MSCs directly diffuse to the CSF, and thus the exosomes containing miR-133b in the CSF, thereby directly reflect those produced by the MSCs. In addition, we cannot exclude the possibility that MSC exosomes stimulate endogenous miR-133b expression in neurons/astrocytes, and are subsequently generated and released from these neural cells and thereby also contribute to exosomes in the CSF [67–69]. Further studies are warranted to directly trace the source of miR-133b enhanced exosomes in the CSF after MSC treatment.

The production and composition of MSC released exosomes are affected by stroke and these exosomes mediate the communication of MSCs and neural cells, modify the neural cells and promote the neurite outgrowth, which may enhance functional recovery after stroke. Exosomes are released by most cell types under physiological conditions, and cellular stress conditions also affect the composition of exosomes [69]. Although there is literature showing short-range diffusion of exosomes [70] and a short half-life time in serum due to possible circulation degradation or phagocytic clearance [71, 72], exosomes spread widely in the brain and exogenous exosomes may be used as a delivery vehicle [73, 74]. Development of gene therapy vehicles for diffuse delivery to the brain is one of the major challenges for clinical gene therapy applications. MSCs exhibit a degree of “immune privilege” due to their ability to suppress T-cell-mediated responses for tissue rejection [75]. MSCs escape immune system surveillance and survive in the CNS even after transplantation of allogeneic [75] or xenogeneic MSCs [76]. Because they may provide a continuous source of released exosomes, MSCs are an ideal cell source of exosomes for active biofactor delivery [77–79]. Thus, exogenous application of MSCs transfected with miR-133b or other beneficial miRNAs warrants investigation as a treatment for stroke in rodent models. We expect that exosome delivery of functional miRNAs further promotes neurite outgrowth and functional recovery after stroke compared with naive MSC treatment.

MiRNAs play key roles in development and appropriate axonal path finding, a process which builds the circuitry of the nervous system [80, 81]. In the injured CNS, the glial scar represents a major impediment to axonal regeneration [38, 82, 83]. It is composed of extracellular matrix deposition and astrogliosis (reactive astrocytes) [84]. Reactive astrocytes dramatically express CTGF [85–87], a major inhibitor of axonal growth at injury sites in the CNS in mammals, and its expression is elevated in plaques from stroke patients [88]. The CTGF expression by reactive astrocytes are associated with matrix deposition and postlesional restructuring [86], as well as the glial scar formation in human cerebral infarction [85]. CTGF is a target of miR-133, and it is down-regulated by miR-133 [82, 89]. Our

NIH-PA Author Manuscript

NIH-PA Author Manuscript

NIH-PA Author Manuscript

present data demonstrate that the increase of miR-133b in astrocytes down regulated CTGF expression, which is consistent with our prevous studies that MSC treatment reduced the thickness of the glial scar [35, 38].

Inhibitory ligands bind to growth cone receptors, activating a Rho-family GTPase intracellular signaling pathway that disrupts the actin cytoskeleton inducing growth cone collapse and/or repulsion [90, 91]. The Rho family of small GTPases, like RhoA, is a key regulator of the neuronal morphological development, and adult neuronal structural changes require actin cytoskeleton reorganization [92]. The 3' UTR of RhoA mRNA contains several miRNA (including miR-133b) binding sites which make the miRNA-dependent silencing machinery reasonable [93, 94]. RhoA mRNA is localized to axons and growth cones, and translation of RhoA is required for growth cone collapse elicited by an axonal guidance cue, Semaphorin 3A (Sema3A) [95]. Sema3A-dependent growth cone collapse is abolished by knock-down of axonal RhoA mRNA [81]. In addition to its impact on axon growth and guidance, RhoA also affects dendrite development and plasticity. In studies in mosaic Drosophila brains, RhoA mutant neurons overextended their dendrites [96]. MiR-133 down-regulates RhoA protein expression [98], and then enhances regrowth of the corticospinal tract after spinal cord injury [99]. RhoA distinct localization in synapses and dendrite microtubules has been confirmed by immunohistochemical analyses and electron microscopy [97]. In our present study, RhoA expression was down-regulated by the over-expression of miR-133b which stimulates neurite outgrowth and improves functional recovery.

In HEK293T cells, over-expression of miR-146a selectively enhanced export of miR146a, and did not alter the relative expression of endogenous and extracellular particle miRNAs [98]. Even so, we cannot exclude the possibility that regulation of other miRNAs within the MSCs and their export via exosomes may be affected by miR-133b over-expression. The miRNA regulation is a network system [13, 99], and the transcription of miRNAs may be regulated [100, 101]. CTGF and RhoA expression may also be controlled by other miRNAs in the neural cells affected by the transfer of miR-133b. As a proof-of-concept study, we need to simplify the target. However, the effects of MSC miR-133b over-expression upon MSC exosome content and miRNAs changes in the recipient cells warrant further study.

Conclusion

MiR-133b in the exosomes released from MSCs post stroke are transferred to neural cells, which regulate gene expression, promote neurite remodeling and improve functional recovery in rats subjected to MCAo.

Supplementary Material

Refer to Web version on PubMed Central for supplementary material.

Acknowledgments

This work was supported by NIH grants R01 AG037506 (MC), R01 NS66041 (YL). We thank Cindi Roberts, Qinge Lu and Sue Santra for technical assistance on histology.

References

1. Fiore R, Siegel G, Schratt G. MicroRNA function in neuronal development, plasticity and disease. Biochim Biophys Acta. 2008; 1779:471–478. [PubMed: 18194678]
2. Zhang B, Wang Q, Pan X. MicroRNAs and their regulatory roles in animals and plants. J Cell Physiol. 2007; 210:279–289. [PubMed: 17096367]

NIH-PA Author Manuscript

NIH-PA Author Manuscript

NIH-PA Author Manuscript

3. Bartel DP. MicroRNAs: genomics, biogenesis, mechanism, and function. Cell. 2004; 116:281–297. [PubMed: 14744438]
4. Zhang B, Pan X, Cobb GP, et al. Plant microRNA: a small regulatory molecule with big impact. Dev Biol. 2006; 289:3–16. [PubMed: 16325172]
5. Lewis BP, Burge CB, Bartel DP. Conserved seed pairing, often flanked by adenosines, indicates that thousands of human genes are microRNA targets. Cell. 2005; 120:15–20. [PubMed: 15652477]
6. Friedman RC, Farh KK, Burge CB, et al. Most mammalian mRNAs are conserved targets of microRNAs. Genome research. 2009; 19:92–105. [PubMed: 18955434]
7. Lim LP, Lau NC, Weinstein EG, et al. The microRNAs of Caenorhabditis elegans. Genes & development. 2003; 17:991–1008. [PubMed: 12672692]
8. Lim LP, Lau NC, Garrett-Engele P, et al. Microarray analysis shows that some microRNAs downregulate large numbers of target mRNAs. Nature. 2005; 433:769–773. [PubMed: 15685193]
9. Brennecke J, Hipfner DR, Stark A, et al. bantam encodes a developmentally regulated microRNA that controls cell proliferation and regulates the proapoptotic gene hid in Drosophila. Cell. 2003; 113:25–36. [PubMed: 12679032]
10. Cuellar TL, McManus MT. MicroRNAs and endocrine biology. The Journal of endocrinology. 2005; 187:327–332. [PubMed: 16423811]
11. Chen CZ, Li L, Lodish HF, et al. MicroRNAs modulate hematopoietic lineage differentiation. Science. 2004; 303:83–86. [PubMed: 14657504]
12. Harfe BD, McManus MT, Mansfield JH, et al. The RNaseIII enzyme Dicer is required for morphogenesis but not patterning of the vertebrate limb. Proc Natl Acad Sci U S A. 2005; 102:10898–10903. [PubMed: 16040801]
13. Olde Loohuis NF, Kos A, Martens GJ, et al. MicroRNA networks direct neuronal development and plasticity. Cell Mol Life Sci. 2012; 69:89–102. [PubMed: 21833581]
14. Saba R, Schratt GM. MicroRNAs in neuronal development, function and dysfunction. Brain Res. 2010; 1338:3–13. [PubMed: 20380818]
15. Costa-Mattioli M, Sossin WS, Klann E, et al. Translational control of long-lasting synaptic plasticity and memory. Neuron. 2009; 61:10–26. [PubMed: 19146809]
16. Ziu M, Fletcher L, Rana S, et al. Temporal differences in microRNA expression patterns in astrocytes and neurons after ischemic injury. PLoS One. 2011; 6:e14724. [PubMed: 21373187]
17. Sethi P, Lukiw WJ. Micro-RNA abundance and stability in human brain: specific alterations in Alzheimer's disease temporal lobe neocortex. Neurosci Lett. 2009; 459:100–104. [PubMed: 19406203]
18. Kocerha J, Kauppinen S, Wahlestedt C. microRNAs in CNS disorders. Neuromolecular Med. 2009; 11:162–172. [PubMed: 19536656]
19. Dogini DB, Ribeiro PA, Rocha C, et al. MicroRNA expression profile in murine central nervous system development. J Mol Neurosci. 2008; 35:331–337. [PubMed: 18452032]
20. Bak M, Silahtaroglu A, Moller M, et al. MicroRNA expression in the adult mouse central nervous system. RNA (New York, N.Y. 2008; 14:432–444.
21. Kapsimali M, Kloosterman WP, de Bruijn E, et al. MicroRNAs show a wide diversity of expression profiles in the developing and mature central nervous system. Genome biology. 2007; 8:R173. [PubMed: 17711588]
22. Mor E, Cabilly Y, Goldshmit Y, et al. Species-specific microRNA roles elucidated following astrocyte activation. Nucleic acids research. 2011; 39:3710–3723. [PubMed: 21247879]
23. Liu NK, Xu XM. MicroRNA in central nervous system trauma and degenerative disorders. Physiological genomics. 2011; 43:571–580. [PubMed: 21385946]
24. Goldie BJ, Cairns MJ. Post-transcriptional trafficking and regulation of neuronal gene expression. Mol Neurobiol. 2012; 45:99–108. [PubMed: 22167484]
25. Zomer A, Vendrig T, Hopmans ES, et al. Exosomes: Fit to deliver small RNA. Communicative & integrative biology. 2010; 3:447–450. [PubMed: 21057637]
26. Pegtel DM, Cosmopoulos K, Thorley-Lawson DA, et al. Functional delivery of viral miRNAs via exosomes. Proc Natl Acad Sci U S A. 2010; 107:6328–6333. [PubMed: 20304794]

NIH-PA Author Manuscript

NIH-PA Author Manuscript

NIH-PA Author Manuscript

27. Katakowski M, Buller B, Wang X, et al. Functional microRNA is transferred between glioma cells. Cancer Res. 2010; 70:8259–8263. [PubMed: 20841486]
28. Lotvall J, Valadi H. Cell to cell signalling via exosomes through esRNA. Cell adhesion & migration. 2007; 1:156–158. [PubMed: 19262134]
29. Smalheiser NR. Exosomal transfer of proteins and RNAs at synapses in the nervous system. Biology direct. 2007; 2:35. [PubMed: 18053135]
30. Record M, Subra C, Silvente-Poirot S, et al. Exosomes as intercellular signalosomes and pharmacological effectors. Biochem Pharmacol. 2011; 81:1171–1182. [PubMed: 21371441]
31. Mathivanan S, Ji H, Simpson RJ. Exosomes: extracellular organelles important in intercellular communication. Journal of proteomics. 2010; 73:1907–1920. [PubMed: 20601276]
32. Valadi H, Ekstrom K, Bossios A, et al. Exosome-mediated transfer of mRNAs and microRNAs is a novel mechanism of genetic exchange between cells. Nature cell biology. 2007; 9:654–659.
33. Chen J, Li Y, Wang L, et al. Therapeutic benefit of intravenous administration of bone marrow stromal cells after cerebral ischemia in rats. Stroke. 2001; 32:1005–1011. [PubMed: 11283404]
34. Chen J, Zhang ZG, Li Y, et al. Intravenous administration of human bone marrow stromal cells induces angiogenesis in the ischemic boundary zone after stroke in rats. Circ Res. 2003; 92:692–699. [PubMed: 12609969]
35. Li Y, Chen J, Zhang CL, et al. Gliosis and brain remodeling after treatment of stroke in rats with marrow stromal cells. Glia. 2005; 49:407–417. [PubMed: 15540231]
36. Caplan AI, Dennis JE. Mesenchymal stem cells as trophic mediators. Journal of cellular biochemistry. 2006; 98:1076–1084. [PubMed: 16619257]
37. Chang YC, Shyu WC, Lin SZ, et al. Regenerative therapy for stroke. Cell Transplant. 2007; 16:171–181. [PubMed: 17474298]
38. Shen LH, Li Y, Gao Q, et al. Down-regulation of neurocan expression in reactive astrocytes promotes axonal regeneration and facilitates the neurorestorative effects of bone marrow stromal cells in the ischemic rat brain. Glia. 2008; 56:1747–1754. [PubMed: 18618668]
39. Dharmasaroja P. Bone marrow-derived mesenchymal stem cells for the treatment of ischemic stroke. J Clin Neurosci. 2009; 16:12–20. [PubMed: 19017556]
40. Liu Z, Li Y, Zhang RL, et al. Bone marrow stromal cells promote skilled motor recovery and enhance contralesional axonal connections after ischemic stroke in adult mice. Stroke. 2011; 42:740–744. [PubMed: 21307396]
41. Xin H, Li Y, Buller B, et al. Exosome Mediated Transfer of miR-133b from Multipotent Mesenchymal Stromal Cells to Neural Cells Contributes to Neurite Outgrowth. Stem Cells. 2012
42. Baddoo M, Hill K, Wilkinson R, et al. Characterization of mesenchymal stem cells isolated from murine bone marrow by negative selection. Journal of cellular biochemistry. 2003; 89:1235–1249. [PubMed: 12898521]
43. Meirelles Lda S, Nardi NB. Murine marrow-derived mesenchymal stem cell: isolation, in vitro expansion, and characterization. British journal of haematology. 2003; 123:702–711. [PubMed: 14616976]
44. Tropel P, Noel D, Platet N, et al. Isolation and characterisation of mesenchymal stem cells from adult mouse bone marrow. Exp Cell Res. 2004; 295:395–406. [PubMed: 15093739]
45. Schallert T, Whishaw IQ. Bilateral cutaneous stimulation of the somatosensory system in hemidecorticate rats. Behav Neurosci. 1984; 98:518–540. [PubMed: 6539617]
46. Zhang L, Zhang RL, Wang Y, et al. Functional recovery in aged and young rats after embolic stroke: treatment with a phosphodiesterase type 5 inhibitor. Stroke. 2005; 36:847–852. [PubMed: 15746452]
47. Zhang L, Zhang ZG, Zhang RL, et al. Effects of a selective CD11b/CD18 antagonist and recombinant human tissue plasminogen activator treatment alone and in combination in a rat embolic model of stroke. Stroke. 2003; 34:1790–1795. [PubMed: 12805500]
48. Lakshmipathy U, Hart RP. Concise review: MicroRNA expression in multipotent mesenchymal stromal cells. Stem Cells. 2008; 26:356–363. [PubMed: 17991914]

NIH-PA Author Manuscript NIH-PA Author Manuscript NIH-PA Author Manuscript

49. Wang S, Cesca F, Loers G, et al. Synapsin I is an oligomannose-carrying glycoprotein, acts as an oligomannose-binding lectin, and promotes neurite outgrowth and neuronal survival when released via glia-derived exosomes. J Neurosci. 2011; 31:7275–7290. [PubMed: 21593312]
50. Pols MS, Klumperman J. Trafficking and function of the tetraspanin CD63. Exp Cell Res. 2009; 315:1584–1592. [PubMed: 18930046]
51. Suetsugu A, Honma K, Saji S, et al. Imaging exosome transfer from breast cancer cells to stroma at metastatic sites in orthotopic nude mouse models. Advanced drug delivery reviews. 2012
52. Lai RC, Arslan F, Lee MM, et al. Exosome secreted by MSC reduces myocardial ischemia/reperfusion injury. Stem cell research. 2010; 4:214–222. [PubMed: 20138817]
53. Guescini M, Genedani S, Stocchi V, et al. Astrocytes and Glioblastoma cells release exosomes carrying mtDNA. J Neural Transm. 2010; 117:1–4. [PubMed: 19680595]
54. Atay S, Gercel-Taylor C, Kesimer M, et al. Morphologic and proteomic characterization of exosomes released by cultured extravillous trophoblast cells. Exp Cell Res. 2011; 317:1192–1202. [PubMed: 21276792]
55. Orozco AF, Lewis DE. Flow cytometric analysis of circulating microparticles in plasma. Cytometry A. 2010; 77:502–514. [PubMed: 20235276]
56. Liu X, Wang HW. Single particle electron microscopy reconstruction of the exosome complex using the random conical tilt method. J Vis Exp. 2011
57. Voelker CC, Garin N, Taylor JS, et al. Selective neurofilament (SMI-32, FNP-7 and N200) expression in subpopulations of layer V pyramidal neurons in vivo and in vitro. Cereb Cortex. 2004; 14:1276–1286. [PubMed: 15166101]
58. Lee VM, Otvos L Jr. Carden MJ, et al. Identification of the major multiphosphorylation site in mammalian neurofilaments. Proc Natl Acad Sci U S A. 1988; 85:1998–2002. [PubMed: 2450354]
59. Calhoun ME, Jucker M, Martin LJ, et al. Comparative evaluation of synaptophysin-based methods for quantification of synapses. J Neurocytol. 1996; 25:821–828. [PubMed: 9023727]
60. Li Y, Sharov VG, Jiang N, et al. Ultrastructural and light microscopic evidence of apoptosis after middle cerebral artery occlusion in the rat. Am J Pathol. 1995; 146:1045–1051. [PubMed: 7747798]
61. Paxinos, G. San Diego: Academic Press; 1995. The Rat nervous system; p. 1136xvii
62. Seyfried DM, Han Y, Yang D, et al. Erythropoietin promotes neurological recovery after intracerebral haemorrhage in rats. Int J Stroke. 2009; 4:250–256. [PubMed: 19689750]
63. Lu M, Chen J, Lu D, et al. Global test statistics for treatment effect of stroke and traumatic brain injury in rats with administration of bone marrow stromal cells. J Neurosci Methods. 2003; 128:183–190. [PubMed: 12948561]
64. Julie M, LEGLER ML, Louise MRYAN. Efficiency and power of tests for multiple binary outcomes. Journal of the American Statistical Association. 1995; 90:14.
65. Liu Z, Li Y, Zhang ZG, et al. Bone marrow stromal cells enhance inter- and intracortical axonal connections after ischemic stroke in adult rats. J Cereb Blood Flow Metab. 2010; 30:1288–1295. [PubMed: 20125183]
66. Niehage C, Steenblock C, Pursche T, et al. The cell surface proteome of human mesenchymal stromal cells. PLoS ONE. 2011; 6:e20399. [PubMed: 21637820]
67. Chen J, Li Y, Katakowski M, et al. Intravenous bone marrow stromal cell therapy reduces apoptosis and promotes endogenous cell proliferation after stroke in female rat. J Neurosci Res. 2003; 73:778–786. [PubMed: 12949903]
68. Shen LH, Li Y, Chen J, et al. Therapeutic benefit of bone marrow stromal cells administered 1 month after stroke. J Cereb Blood Flow Metab. 2007; 27:6–13. [PubMed: 16596121]
69. Eldh M, Ekstrom K, Valadi H, et al. Exosomes communicate protective messages during oxidative stress; possible role of exosomal shuttle RNA. PLoS ONE. 2010; 5:e15353. [PubMed: 21179422]
70. Montecalvo A, Shufesky WJ, Stolz DB, et al. Exosomes as a short-range mechanism to spread alloantigen between dendritic cells during T cell allorecognition. J Immunol. 2008; 180:3081–3090. [PubMed: 18292531]
71. Fitzner D, Schnaars M, van Rossum D, et al. Selective transfer of exosomes from oligodendrocytes to microglia by macropinocytosis. J Cell Sci. 2011; 124:447–458. [PubMed: 21242314]

NIH-PA Author Manuscript

NIH-PA Author Manuscript

NIH-PA Author Manuscript

72. MacKay PA, Leibundgut-Landmann S, Koch N, et al. Circulating, soluble forms of major histocompatibility complex antigens are not exosome-associated. European journal of immunology. 2006; 36:2875–2884. [PubMed: 17072917]
73. Bakhti M, Winter C, Simons M. Inhibition of myelin membrane sheath formation by oligodendrocyte-derived exosome-like vesicles. J Biol Chem. 2011; 286:787–796. [PubMed: 20978131]
74. Lai CP, Breakefield XO. Role of Exosomes/Microvesicles in the Nervous System and Use in Emerging Therapies. Front Physiol. 2012; 3:228. [PubMed: 22754538]
75. Di Nicola M, Carlo-Stella C, Magni M, et al. Human bone marrow stromal cells suppress T-lymphocyte proliferation induced by cellular or nonspecific mitogenic stimuli. Blood. 2002; 99:3838–3843. [PubMed: 11986244]
76. Li Y, McIntosh K, Chen J, et al. Allogeneic bone marrow stromal cells promote glial-axonal remodeling without immunologic sensitization after stroke in rats. Exp Neurol. 2006; 198:313–325. [PubMed: 16455080]
77. Yeo RW, Lai RC, Zhang B, et al. Mesenchymal stem cell: An efficient mass producer of exosomes for drug delivery. Advanced drug delivery reviews. 2012
78. Chen TS, Arslan F, Yin Y, et al. Enabling a robust scalable manufacturing process for therapeutic exosomes through oncogenic immortalization of human ESC-derived MSCs. Journal of translational medicine. 2011; 9:47. [PubMed: 21513579]
79. Lai RC, Yeo RW, Tan KH, et al. Exosomes for drug delivery - a novel application for the mesenchymal stem cell. Biotechnol Adv. 2012
80. Giraldez AJ, Cinalli RM, Glasner ME, et al. MicroRNAs regulate brain morphogenesis in zebrafish. Science. 2005; 308:833–838. [PubMed: 15774722]
81. Hengst U, Cox LJ, Macosko EZ, et al. Functional and selective RNA interference in developing axons and growth cones. J Neurosci. 2006; 26:5727–5732. [PubMed: 16723529]
82. White RE, Jakeman LB. Don't fence me in: harnessing the beneficial roles of astrocytes for spinal cord repair. Restor Neurol Neurosci. 2008; 26:197–214. [PubMed: 18820411]
83. Wanner IB, Deik A, Torres M, et al. A new in vitro model of the glial scar inhibits axon growth. Glia. 2008
84. Conrad S, Schluesener HJ, Adibzahdeh M, et al. Spinal cord injury induction of lesional expression of profibrotic and angiogenic connective tissue growth factor confined to reactive astrocytes, invading fibroblasts and endothelial cells. Journal of neurosurgery. 2005; 2:319–326. [PubMed: 15796357]
85. Schwab JM, Postler E, Nguyen TD, et al. Connective tissue growth factor is expressed by a subset of reactive astrocytes in human cerebral infarction. Neuropathol Appl Neurobiol. 2000; 26:434–440. [PubMed: 11054183]
86. Hertel M, Tretter Y, Alzheimer C, et al. Connective tissue growth factor: a novel player in tissue reorganization after brain injury? Eur J Neurosci. 2000; 12:376–380. [PubMed: 10651893]
87. Schwab JM, Beschorner R, Nguyen TD, et al. Differential cellular accumulation of connective tissue growth factor defines a subset of reactive astrocytes, invading fibroblasts, and endothelial cells following central nervous system injury in rats and humans. J Neurotrauma. 2001; 18:377–388. [PubMed: 11336439]
88. Leeuwis JW, Nguyen TQ, Theunissen MG, et al. Connective tissue growth factor is associated with a stable atherosclerotic plaque phenotype and is involved in plaque stabilization after stroke. Stroke. 2010; 41:2979–2981. [PubMed: 20966418]
89. Duisters RF, Tijsen AJ, Schroen B, et al. miR-133 and miR-30 regulate connective tissue growth factor: implications for a role of microRNAs in myocardial matrix remodeling. Circ Res. 2009; 104:170–178. 176p following 178. [PubMed: 19096030]
90. Walmsley AR, Mir AK. Targeting the Nogo-A signalling pathway to promote recovery following acute CNS injury. Curr Pharm Des. 2007; 13:2470–2484. [PubMed: 17692015]
91. Lee JK, Kim JE, Sivula M, et al. Nogo receptor antagonism promotes stroke recovery by enhancing axonal plasticity. J Neurosci. 2004; 24:6209–6217. [PubMed: 15240813]
92. Hall A, Lalli G. Rho and Ras GTPases in axon growth, guidance, and branching. Cold Spring Harbor perspectives in biology. 2010; 2:a001818. [PubMed: 20182621]

NIH-PA Author Manuscript

NIH-PA Author Manuscript

NIH-PA Author Manuscript

93. Yu YM, Gibbs KM, Davila J, et al. MicroRNA miR-133b is essential for functional recovery after spinal cord injury in adult zebrafish. Eur J Neurosci. 2011; 33:1587–1597. [PubMed: 21447094]

94. Qin W, Dong P, Ma C, et al. MicroRNA-133b is a key promoter of cervical carcinoma development through the activation of the ERK and AKT1 pathways. Oncogene. 2011

95. Wu KY, Hengst U, Cox LJ, et al. Local translation of RhoA regulates growth cone collapse. Nature. 2005; 436:1020–1024. [PubMed: 16107849]

96. Lee T, Winter C, Marticke SS, et al. Essential roles of Drosophila RhoA in the regulation of neuroblast proliferation and dendritic but not axonal morphogenesis. Neuron. 2000; 25:307–316. [PubMed: 10719887]

97. Huesa G, Baltrons MA, Gomez-Ramos P, et al. Altered distribution of RhoA in Alzheimer's disease and AbetaPP overexpressing mice. J Alzheimers Dis. 2010; 19:37–56. [PubMed: 20061625]

98. Guduric-Fuchs J, A OC, Camp B, et al. Selective extracellular vesicle-mediated export of an overlapping set of microRNAs from multiple cell types. BMC Genomics. 2012; 13:357. [PubMed: 22849433]

99. Gao FB. Posttranscriptional control of neuronal development by microRNA networks. Trends Neurosci. 2008; 31:20–26. [PubMed: 18054394]

100. O'Carroll D, Schaefer A. General Principals of miRNA Biogenesis Regulation in the Brain. Neuropsychopharmacology. 2012

101. Kim VN, Nam JW. Genomics of microRNA. Trends Genet. 2006; 22:165–173. [PubMed: 16446010]

102. Nelson PT, Baldwin DA, Kloosterman WP, et al. RAKE and LNA-ISH reveal microRNA expression and localization in archival human brain. RNA New York, N.Y. 2006; 12:187–191.

103. Kloosterman WP, Wienholds E, de Bruijn E, et al. In situ detection of miRNAs in animal embryos using LNA-modified oligonucleotide probes. Nat Methods. 2006; 3:27–29. [PubMed: 16369549]

NIH-PA Author Manuscript
NIH-PA Author Manuscript
NIH-PA Author Manuscript

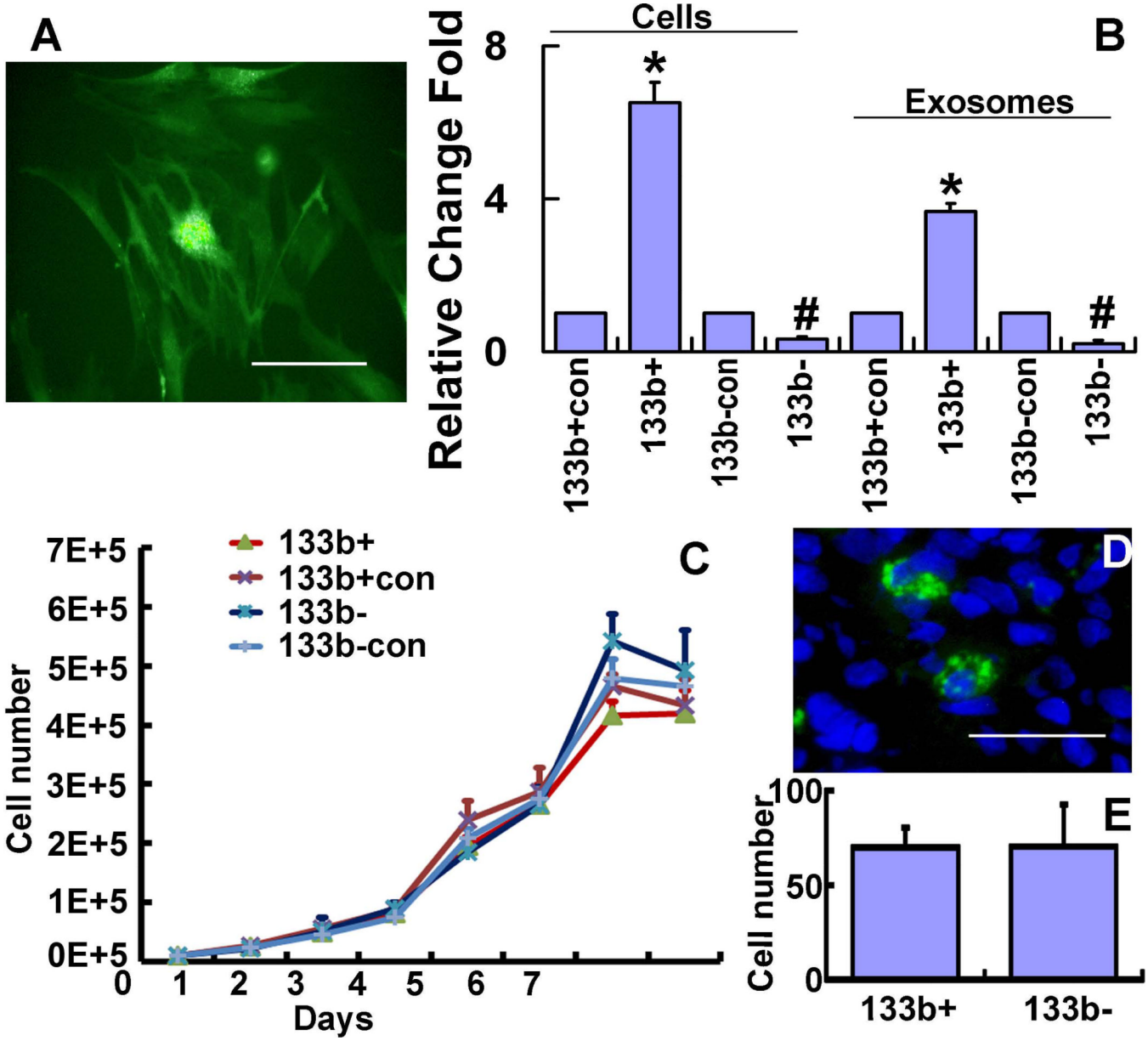

Figure 1.

Specific lentiviruses modify MSC miR-133b expression. Puromycin selected stable MSC cell lines infected with LentimiRa-GFP-hsa-mir-133b lentivirus (miR-133b^{+}MSC), GFP Blank miRNA/microRNA lentivirus (miR-133b^{+CON}MSC), miRZip-133b anti-miR-133b microRNA lentivirus (miR-133bMSC) and pGreenPuro Scramble Hairpin Control lentivirus (miR-133b^{-CON}MSC), respectively. Green fluorescent protein (GFP) was used to monitor the infection efficiency (A). RT-PCR data show the miR-133b expression level in miR-133b^{+}MSCs and their exosomes were significantly increased compared to those in miR-133b^{+CON}MSCs; however, miR-133bMSCs exhibited significantly decreased the miR-133b expression level in cells and exosomes compared to those in miR-133b^{-CON}MSCs (B). Growth curve analysis shows that miR-133b^{+}MSCs and miR-133bMSCs and their corresponding control MSCs exhibit similar cell proliferation character(C). The data of counting GFP tag positive cells show that miR-133b^{+}MSCs and miR-133bMSCs have similar characters on survival and trafficking to brain (D,E). 133b

NIH-PA Author Manuscript

NIH-PA Author Manuscript

NIH-PA Author Manuscript

+con: miR-133b^{+CON}MSCs, 133b+: miR-133b^{+}MSCs, 133b-con: miR-133b^{-CON}MSCs, 133b-: miR-133bMSCs. *P<0.01 compared with miR-133b^{+CON}MSCs, respectively; #P<0.01 compared with miR-133b^{-CON}MSC, respectively. Scale bar = 50 μm. Mean ± SE, n=3/group (B,C) and n=6/group (D).

NIH-PA Author Manuscript
NIH-PA Author Manuscript
NIH-PA Author Manuscript

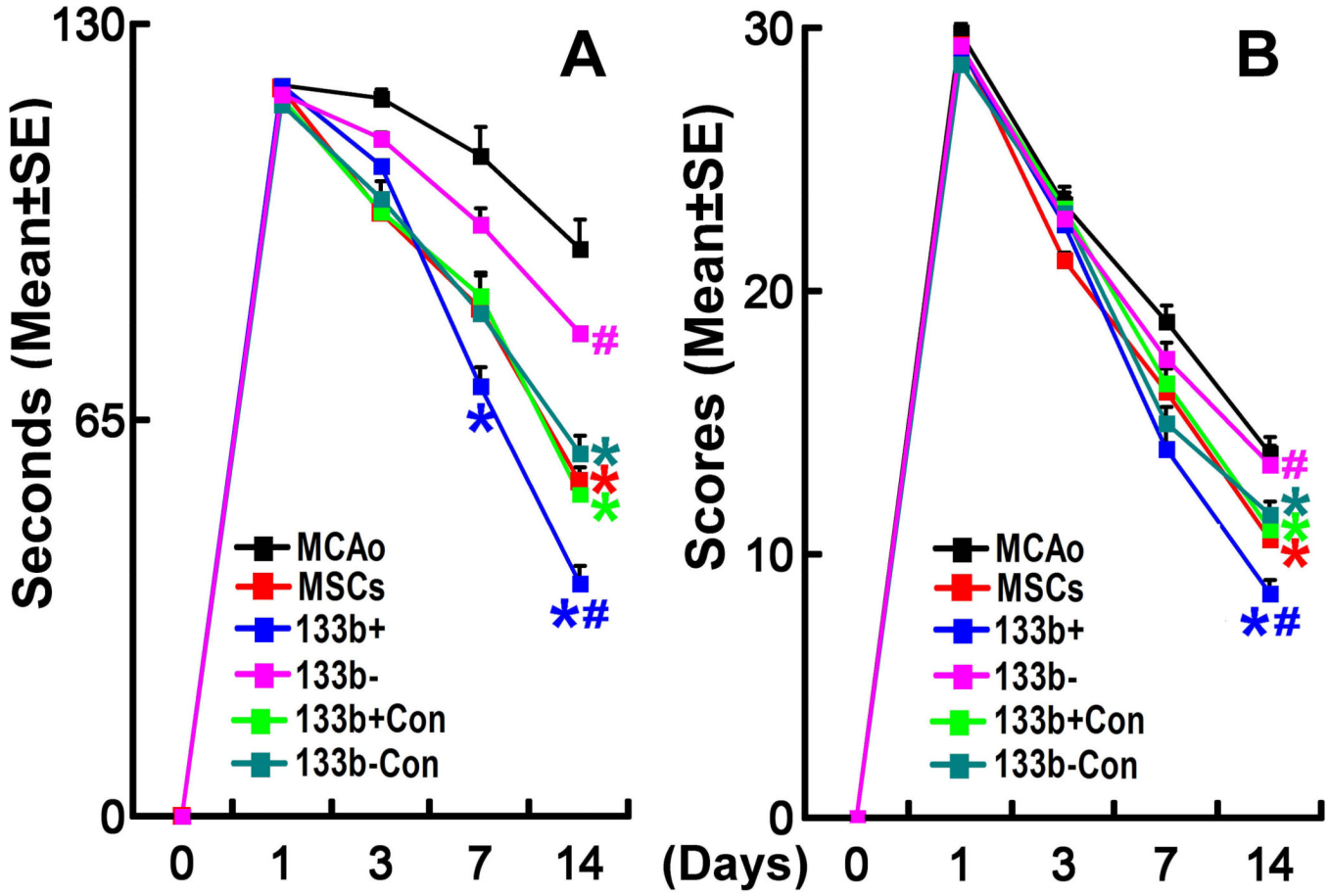

Figure 2.

MiR-133b mediates MSC induced functional recovery. The adhesive-removal test (A) and Foot-fault test (B) were performed prior to the treatment after MCAo (baseline), at day 3 and 7, and at day 14 before sacrifice after MCAo. Compared with PBS treatment, naive MSCs, miR-133b^{+CON}MSCs and miR-133b^{-CON}MSCs significantly improved functional recovery at day 14 after MCAo, while miR-133b^{+}MSCs significantly improved functional recovery at both day 7 (adhesive-removal test only) and 14 after MCAo, and miR-133bMSCs had no obvious beneficial effects at these two time points. Compared with their corresponding control MSC treatment, miR-133b^{+}MSCs significantly improved, while miR-133bMSCs treatment significantly decreased, functional recovery at day 14 after MCAo. MCAo: MCAo rats administered with PBS, MSCs: MCAo rats administered with naive MSCs, 133b+: MCAo rats administered with miR-133b^{+}MSCs, 133b+con: MCAo rats administered with miR-133b^{+CON}MSCs, 133b-: MCAo rats administered with miR-133bMSCs, 133b-con: MCAo rats administered with miR-133b^{-CON}MSCs. Respective color * in A and B indicates $P<0.05$, compared with PBS treatment; respective color # in A and B indicates $P<0.05$, compared with their corresponding control MSC treatment. Mean ± SE, n=6/group.

NIH-PA Author Manuscript
NIH-PA Author Manuscript
NIH-PA Author Manuscript

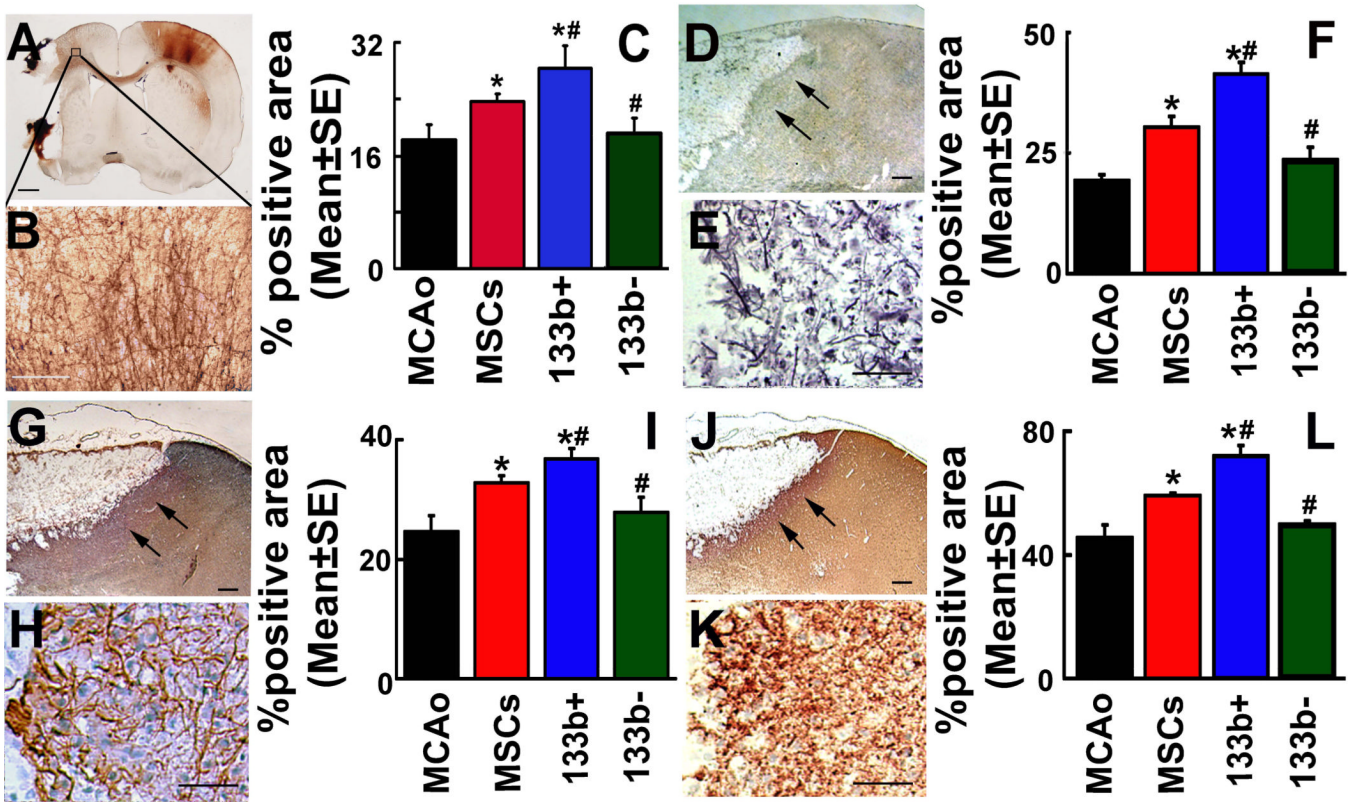

Figure 3.

MiR-133b increases axonal plasticity and neurite remodeling in the IBZ. A representative image shows the BDA-positive labeling in a rat vobratome coronal brain section (A). The BDA labeled axons in the CFA which ipsilateral to the lesion were enlarged in B. Analysis data (C) show that intracortical axonal density was significantly increased after naive MSC treatment compared with PBS treatment at day 14 after MCAo. MiR-133b^{+}MSC treatment significantly increased while miR-133bMSC treatment significantly decreased the cortical axonal density at day 14 after MCAo compared with naive MSC treatment ($P<0.05$, C). Bielshowsky silver staining, NF-200 and synaptophysin immunostaining performed on adjacent frozen coronal brain sections to detect the neurite remodeling. Arrows indicate Bielshowsky silver (D), NF-200 (G) and synaptophysin (J) staining in the IBZ, respectively, of the ipsilateral cortex (E, H and K are enlarged from D, G, and J, respectively). Compared with PBS treatment, the positive staining of Bielshowsky silver, NF-200 and synaptophysin significantly increased at day 14 after MCAo along the IBZ after naive MSC treatment. MiR-133b^{+}MSC treatment significantly increased, while miR-133bMSC treatment significantly decreased the positive staining area of Bielshowsky silver, NF-200 and synaptophysin at day 14 after MCAo compared with naive MSC treatment. MCAo: MCAo rats administered with PBS, MSCs: MCAo rats administered with naive MSCs, 133b+: MCAo rats administered with miR-133b^{+}MSCs, 133b-: MCAo rats administered with miR-133bMSCs. *$P<0.05$ compared with MCAo control; #$P<0.05$ compared with naive MSCs. Scale bar = 1mm in A and 250 μm in B, 50 μm of the rest, Mean ± SE, n=3/group (C). n=6/group (F, I and L).

NIH-PA Author Manuscript

NIH-PA Author Manuscript

NIH-PA Author Manuscript

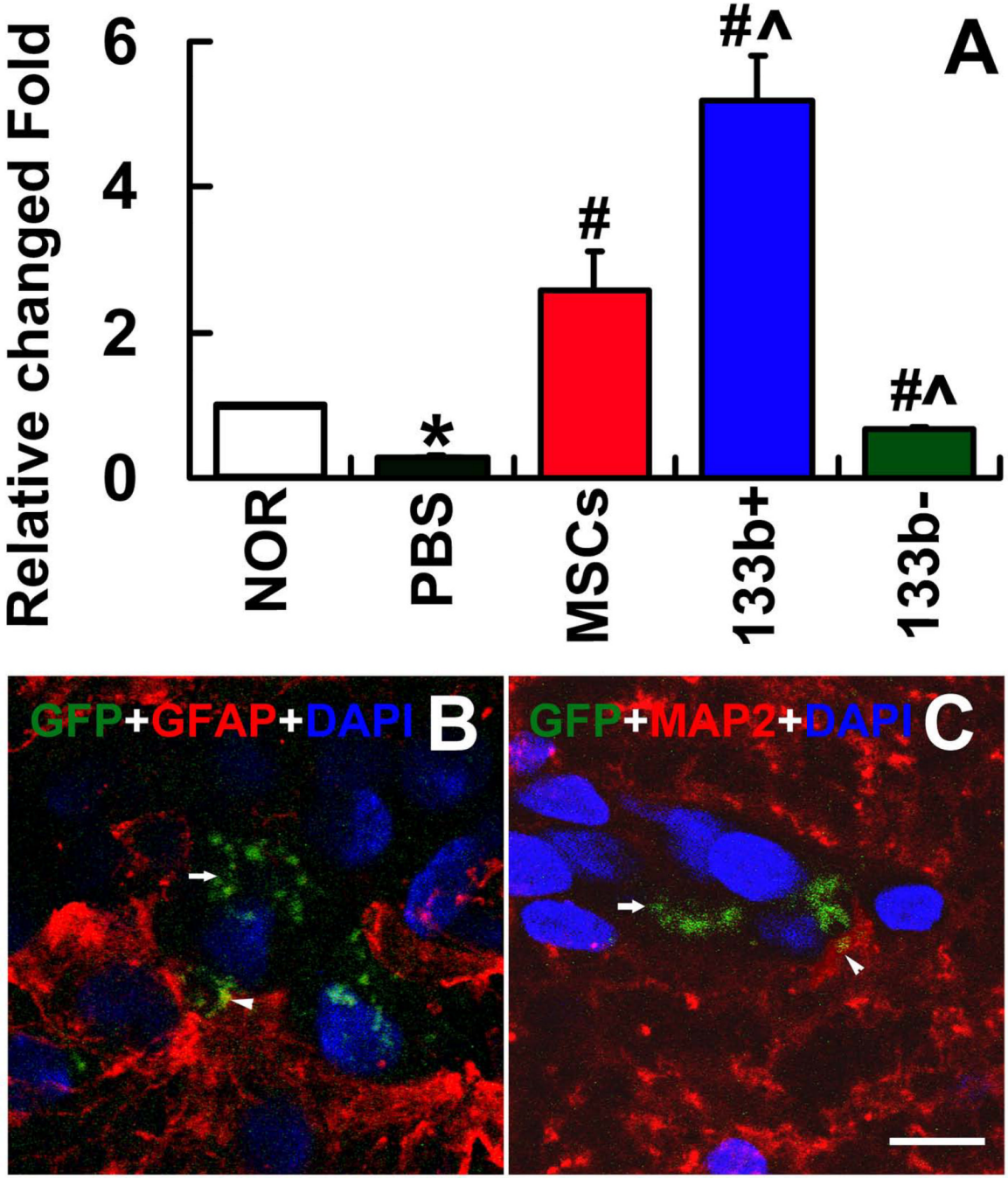

Figure 4.

MiR-133b levels in CSF exosomes and MSC exosomes communicated with astrocytes and neurons. RT-PCR was employed to measure the miR-133b level in exosomes collected from the CSF at day 14 after MCAo. Data show that MCAo decreased the miR-133b level in the CSF exosomes. The miR-133b level in the CSF exosomes was significantly increased compared to the MCAo control after treatment with naive MSCs. MiR-133b^{+}MSC treatment significantly increased, while miR-133bMSC treatment significantly decreased miR-133b levels in the CSF exosomes, respectively, compared with the naive MSC treatment (A). B–C show that exosomes-enriched particles of MSCs (arrows) in the IBZ and taken up by adjacent astrocytes and neurons (arrow heads). NOR: Normal rats, PBS: MCAo rats

NIH-PA Author Manuscript

NIH-PA Author Manuscript

NIH-PA Author Manuscript

administered with PBS, MSCs: MCAo rats administered with naive MSCs, 133b+: MCAo rats administered with miR-133b^{+}MSCs, 133b-: MCAo rats administered with miR-133bMSCs. *P<0.05 compared with NOR; #P<0.05 compared with PBS; ^P<0.05 compared with MSCs. Mean±SE, n=3/group.

NIH-PA Author Manuscript
NIH-PA Author Manuscript
NIH-PA Author Manuscript

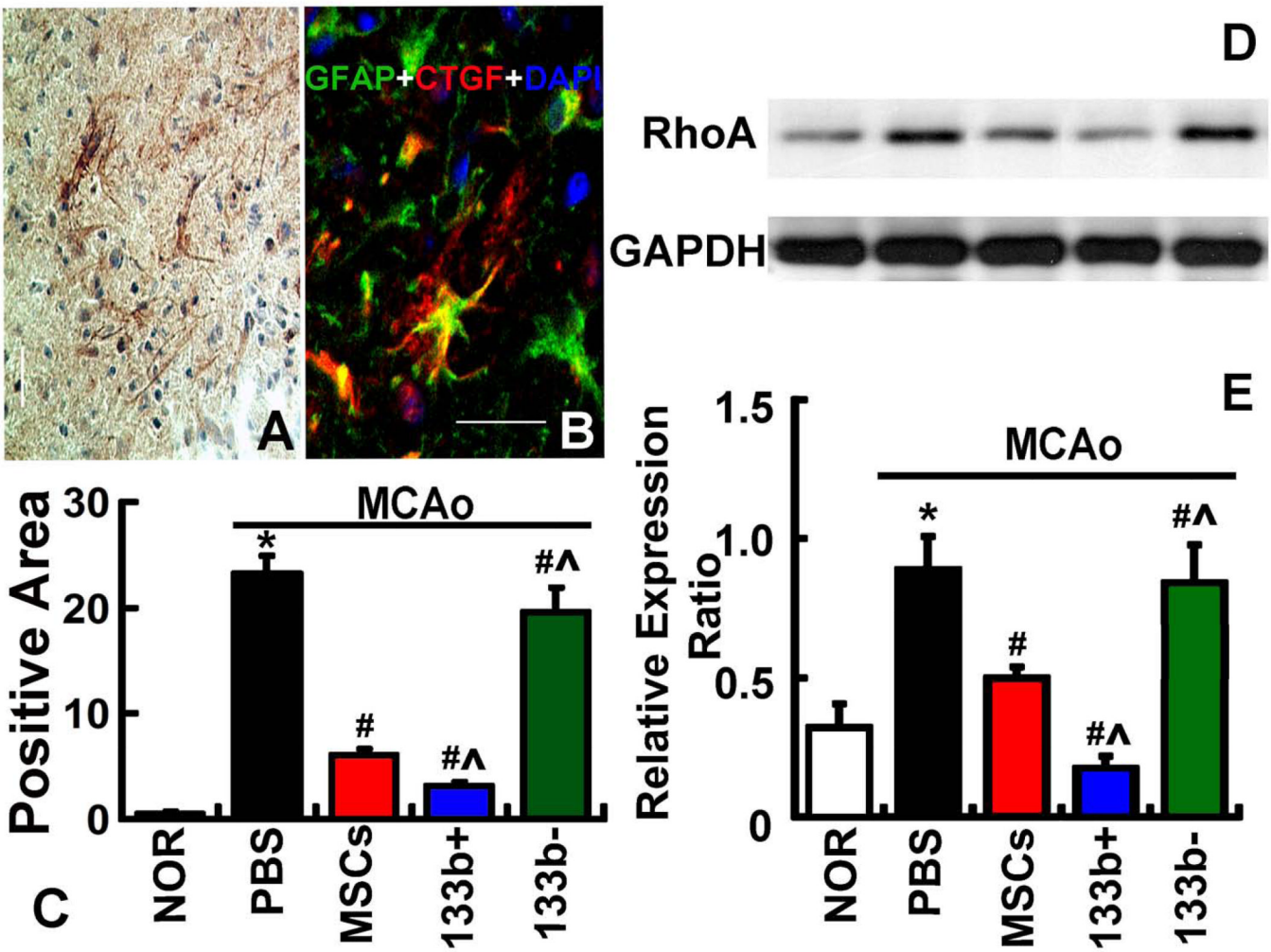

Figure 5.

MiR-133b regulates CTGF expression in astrocytes and RhoA expression in the IBZ. Immunostaining shows CTGF expression in the IBZ (A) and colocalized with GFAP in astrocytes (B). Immunostaining analysis data (C) show that CTGF expression significantly increased at day 14 after MCAo compared with normal rats. The administration of naive MSCs significantly decreased the CTGF expression at day 14 after MCAo, compared with MCAo alone rats. MiR-133b^{+}MSC treatment further significantly decreased CTFG at day 14 after MCAo compared with naïve MSC treatment, while the CTGF expression in miR-133b^{-}MSC treatment was sustained at a significantly elevated level at day 14 after MCAo compared with naïve MSC treatment. Western blot was used to detect the RhoA level in the IBZ (D). The data (E) show that RhoA expression significantly increased at day 14 after MCAo compared with normal rats. Naive MSC treatment significantly decreased the RhoA expression at day 14 after MCAo, compared with MCAo alone rats. MiR-133b^{+}MSC treatment further significantly decreased RhoA at day 14 after MCAo compared with that naive MSC treatment, and the RhoA expression after miR-133bMSC treatment was sustained at a similar elevated level at day 14 after MCAo compared with that after naive MSC treatment. NOR: Normal rats, PBS: MCAo rats administered with PBS, MSCs: MCAo rats administered with naive MSCs, 133b+: MCAo rats administered with miR-133b^{+}MSCs, 133b-: MCAo rats administered with miR-133bMSCs. *P<0.05 compared

with NOR; #P<0.05 compared with PBS; ^P<0.05 compared with MSCs. Scale bar = 50 μm. Mean ± SE, n=6/group.

NIH-PA Author Manuscript
NIH-PA Author Manuscript
NIH-PA Author Manuscript